Borane incorporation in a non-fullerene acceptor to tune steric and electronic properties and improve organic solar cell performance

Thomas A. Welsh,[a] Audrey Laventure,[a] Abdullah F. Alahmadi,[b] Guanghui Zhang,[c] Thomas Baumgartner,[a,d] Yingping Zou,[c] Frieder Jäkle,[b]* and Gregory C. Welch[a]*

[a]*Department of Chemistry, University of Calgary, 2500 University Drive N.W., Calgary, AB, T2N 1N4, Canada. E-mail: gregory.welch@ucalgary.ca*

[b]*Department of Chemistry, Rutgers University–Newark, 73 Warren Street, Newark, New Jersey 07102, USA.*

[c]*College of Chemistry and Chemical Engineering, Central South University, Changsha 410083, China.*

[d]*Department of Chemistry, York University, 4700 Keele St, Toronto, ON, Canada M3J 1P3.*

Supporting Information (SI): Experimental details. Details on cyclic voltammetry, optical absorption and emission spectroscopy, differential scanning calorimetry, thermal gravimetric analysis, device fabrication and AFM characterization. See DOI: 10.1039/x0xx00000x

Abstract

Herein we study the effects of borane incorporation into a perylene diimide (PDI) based non-fullerene acceptor (NFA). We have previously demonstrated that a PDI-bithiophene-PDI ($(PDI)_2Th_2$) compound can be synthesized via direct (hetero)arylation techniques and can be easily modified to incorporate a phosphole in the bithiophene core ($(PDI)_2Th_2PO$ to tune the electronic and geometric properties. In this work we have synthesized the borane analogue ($(PDI)_2Th_2B$) and demonstrate that the organoboron moiety heavily influences the optical, electronic, and geometric properties. To demonstrate what effects borane functionalization has on device performance, green solvent solution processed bulk-heterojunction solar cells were fabricated using a medium gap donor polymer TTFQx-T1 and each PDI compound as the NFA. Devices with the new borane containing compound provided the highest efficiency, more than twice that for the other compounds, which was attributed to a highly twisted structure allowing for a more favorable active-layer morphology to be formed.

Keywords: Borane functionalization, perylene diimide, non-fullerene acceptors, organic photovoltaics, organic materials, green processing conditions.

1. Introduction

Functional π-conjugated organic molecules are an exciting class of semiconducting materials for use as active components in optoelectronic devices.[1] Synthetic versatility, highly tuneable physical, optical, and electronic properties, and the ability to be solution processed into electronically active thin-films at room temperature have made such molecules a hot area of study. Conjugated organic materials have been used in a variety of energy-related applications, such as photovoltaics,[2–5] field-effect transistors,[6–8] and light-emitting devices.[9–11] In order to function in

electronic devices organic materials need to possess appropriate optical and electronic properties. These can be acquired through tuning *via* the incorporation of heteroatoms into a conjugated π-system.

Boron is a versatile element that has been widely used to tailor the properties of organic conjugated materials. In previous decades boron was incorporated into small molecules[12,13] and polymers[14,15] as a side-chain[16] or directly in the polymer backbone[17] (Figure 1A/B). Due to its Lewis acidic nature, tricoordinate boron incorporation has been used to develop sensor materials for various anions such as fluoride.[15,18–21] Due to its vacant p_z orbital, it can be incorporated either as a tricoordinate trigonal planar borane[15] or as a tetracoordinate tetrahedral borate via classic Lewis acid-base interactions.[22] This provides researchers with the ability to tune optoelectronic[23,24] and geometric properties[25] of boron-containing materials.

In conjugated materials, tricoordinate boron lowers the LUMO energy level *via* interaction between the π* and empty B p_z orbital.[26] The vacant B p_z orbital also promotes intramolecular charge transfer (ICT), giving these types of compounds exceptional photophysical properties. The use of tricoordinate borane also provides a degree of flexibility to the polymer or small molecule, as the boron substituents, if they are not too sterically bulky, can freely rotate about the boron bond. Conversely, tetracoordinate borate can be used to fuse the geometry of a polymer or small molecule through intramolecular coordination Lewis acid–base interaction (Figure 1C). This has the effect of planarizing the molecular framework and increasing the conjugation and has been used to improve the performance in polymer solar cells[22,27] and organic field effect transistors.[28]

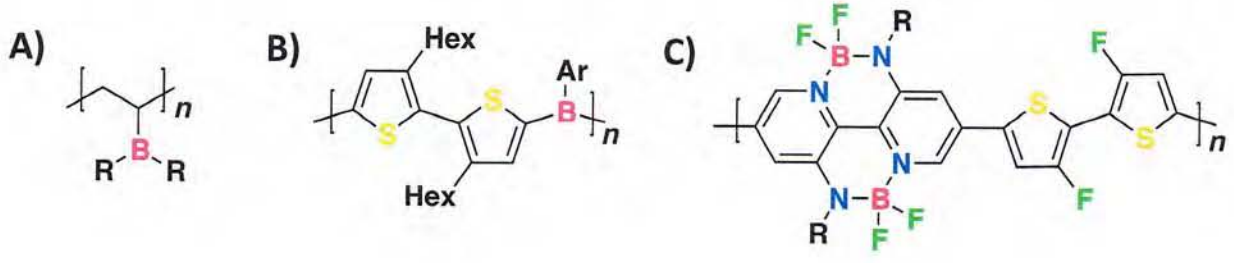

Figure 1: The use of boron in polymers as a borane[14] in A) side chains and B) backbones and C) as a borate.[27] Tricoordinate borane provides a Lewis acidic site, tuning of optoelectronic properties and greater flexibility while tetracoordinate borate formation locks the conjugated backbone reducing conformational disorder.

Our groups are interested in synthesizing and developing new materials for organic electronic applications. Recently, we have focused on synthesizing materials for organic solar cells (OSC), particularly non-fullerene acceptors (NFAs).[29–31] The N-annulated PDI[32] has proved to be quite a useful building block to construct NFAs owing to ease of functionalization,[33] ability to participate in direct (hetero)arylation (DHA) coupling reactions,[34] and high solubility. Materials based on a PDI–π-core–PDI framework have been shown to be effective non-fullerene acceptors (NFA) in bulk heterojunction (BHJ) solar cells.[29,30,35–38]

In the design of NFAs there is ongoing interest in determining whether increased conformational disorder (i.e. 'twisting') in acceptor materials leads to increased performance in OSCs. Recent work by the Yan group involving a PDI tetramer has shown that a fused and more planar system gave OSCs with better performance than its unfused and more twisted analogue.[39] Conversely, the Sun group has shown that a S-annulated PDI tetramer possessed increased twist and led to OSCs with higher performance than the non-annulated less-twisted analogue.[40] In our labs, dimeric N-annulated PDI NFAs with larger dihedral angels between the PDI units have given rise to the best performing OSC devices.[41,42]

Previously, we have functionalized PDI–bithiophene–PDI with phosphorus and shown that the phosphole renders the π-conjugated system more electron-deficient.[35] The incorporation of a phosphanyl or phosphoryl bridge at the 3 and 3' positions of bithiophene has been shown to be a versatile method of functionalization.[43] This forms a fused phosphole system, which has unique

optoelectronic properties compared to unfunctionalized bithiophene.[44–47] Specifically, the incorporation of the phosphole lowers the system's LUMO energy level through interaction between the bithiophene π^* orbital and P–R σ^* orbital.[48] The phosphole bithiophene is also a planar system thereby providing the PDI–bithiophene–PDI framework with a rigid core.

For this study, we wanted to determine if the addition of a borane moiety into PDI–bithiophene–PDI would maintain the electron deficient properties while also allowing for a more flexible core and what the impact would be on OSC performance. When boron has been incorporated in NFAs it is generally found in the tetracoordinate borate form constraining the geometry.[22,27,49] Recent literature has shown that a tetracoordinate organoboron NFA achieved a power conversion efficiency (PCE) of 7%.[50] There are very few examples of tricoordinate boron's use in OSC NFAs. One early example demonstrated the use of an n-type organoboron polymer as an acceptor when paired with the donor P3HT.[51] More recent work has also shown the potential for polymers incorporating borane moieties in the backbone as NFAs in all polymer solar cells with PTB7-Th donor polymer.[31] However, there are no examples of a PDI-based small molecule NFA incorporating borane. This research aims to fill that gap and provide a benchmark compound by which to compare future borane-based NFA materials.

2. Results and Discussion

The three materials studied, displayed in Figure 2, are the unfunctionalized $(PDI)_2Th_2$, phosphoryl-functionalized $(PDI)_2Th_2PO$, and borane-functionalized $(PDI)_2Th_2B$, which is a new material based on bis(thien-2-yl)(2,4,6-tris(trifluoro-methyl)phenyl)borane($(FMes)BTh_2$).[52] Fusion of 2,2'-bithiophene with a phosphoryl moiety in 3,3'-positions results in a planar system. Embedding a trivalent boron center at the 2,2'-position on the other hand adds a flexible three-coordinate building block with an additional bond about which the molecule can rotate, potentially

leading to a more twisted system compared to unfunctionalized 2,2'-bithiophene.[25] The FMes-substituted dithienylborane building block was chosen because of its previously demonstrated highly electron-deficient character.[52] Combination of (FMes)BTh_2 with pyridalthiadiazole groups was shown to result in organoborane Lewis acids with superior fluoride anion binding characteristics,[53] while the combination with isoindigo and diketopyrrolopyrrole groups led to the first examples of polymeric NFAs containing tricoordinate borane moieties.[31]

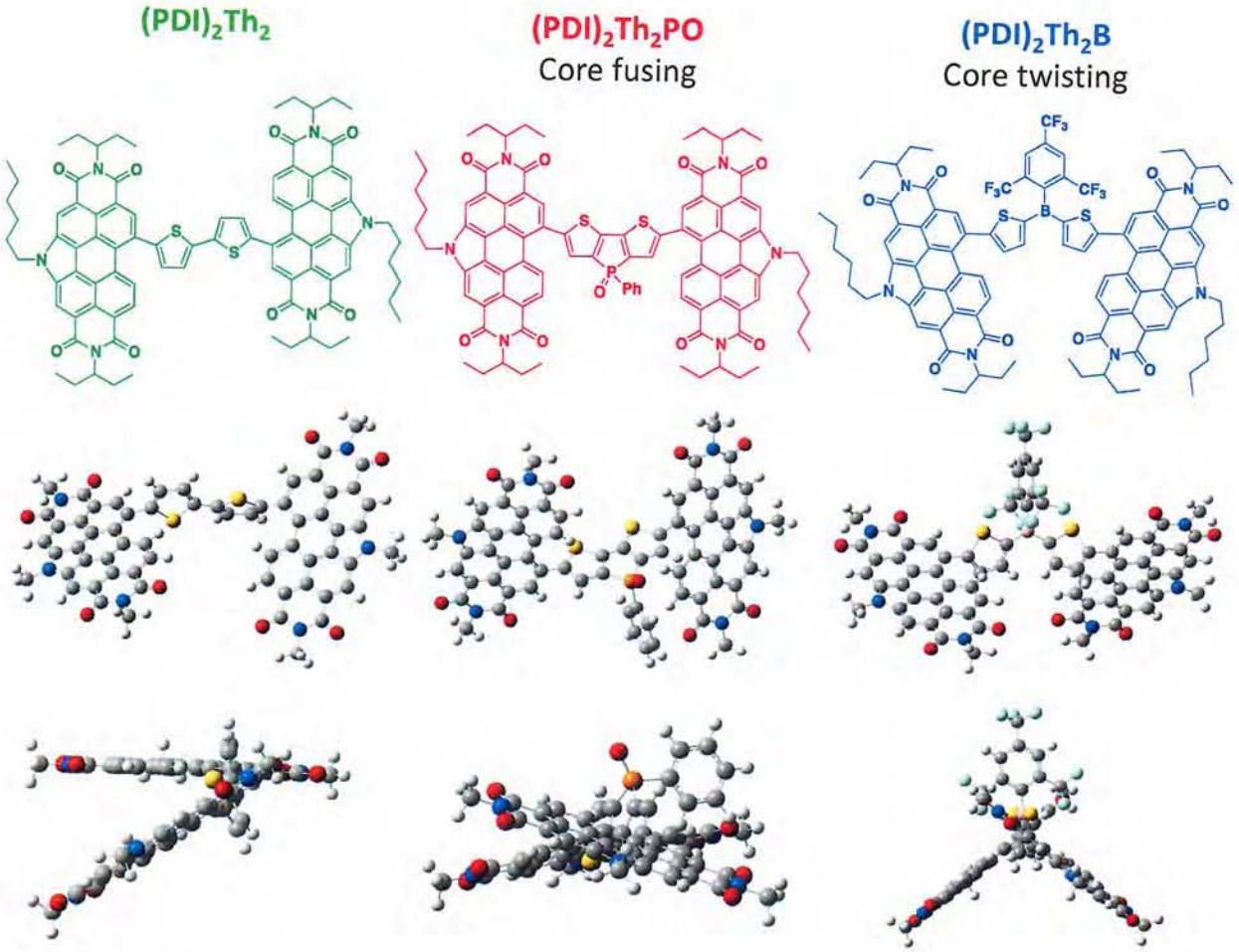

Dihedral			
Th–Th	32°	0°	44°
PDI–Th	96°	104°	97°
PDI–PDI	35°	29°	96°

Figure 2: $(PDI)_2Th_2$ (previous work[41]), $(PDI)_2Th_2PO$ (previous work[35]), and $(PDI)_2Th_2B$ (this work) and the effects of heteroatom substitution on the bithiophene core. Optimized geometry structures are shown with side-on views to show the dihedral angles, listed below. Calculations were performed using Gaussian16[54] input files and results were visualized using GaussView05.[55] All alkyl chains were replaced with a methyl group. The B3LYP[56–58] level of theory with 6-31G(d,p)[59–64] basis set were used for the calculations.

2.1. Molecular geometry calculations

Density functional theory (DFT) calculations can often provide insights into photophysical properties, energy levels, or molecular geometry.[65–67] For this study, since our hypothesis was that functionalization of the bithiophene core would lead to drastically different molecular orientations, we performed geometry optimization calculations using the B3LYP[56–58] level of theory with 6-31G(d,p)[59–64] basis set and analysed the thiophene–thiophene, PDI–thiophene, and PDI–PDI dihedral angles. Both $(PDI)_2Th_2$ and $(PDI)_2Th_2PO$ have previously been studied by DFT calculations.[35,41] The DFT results are displayed in Figure 2 along with dihedral angles. All compounds have large dihedral angles between the PDI and thiophene units. The PDI–PDI dihedral angles on the other hand range from small in $(PDI)_2Th_2$ and $(PDI)_2Th_2PO$ (35° and 29°, respectively) to large in $(PDI)_2Th_2B$ (96°). The thiophene–thiophene dihedrals are 32° in $(PDI)_2Th_2$, 0° in $(PDI)_2Th_2PO$ (as would be expected for a fused bithiophene), and 44° in $(PDI)_2Th_2B$. This is a much larger thiophene–thiophene dihedral angle than previously reported for functionalized $(FMes)BTh_2$ species.[52,53] Combined with the large PDI–PDI dihedral angle, this lends credence to our hypothesis that boron-functionalization of the bithiophene core leads to a more twisted PDI–bithiophene–PDI species than unfunctionalized bithiophene. Furthermore, due to the 120° angles about the trivalent boron centre, it is likely that $(PDI)_2Th_2B$ is less susceptible

of or even prevented from adopting a completely coplanar geometry, and that the PDI–Th units would be optically and electronically isolated from each other. For the fused-core $(PDI)_2Th_2PO$ and even unfunctionalized $(PDI)_2Th_2$, the propensity to form coplanar systems is likely much higher and this would have a large effect on how each species performs in photovoltaic devices.

2.2. Synthesis of $(PDI)_2Th_2B$

Both $(PDI)_2Th_2$ and $(PDI)_2Th_2PO$ were previously synthesized *via* DHA,[35,41] a coupling method that eliminates the need for stochiometric amounts of transmetalation reagents.[68–70] This makes DHA much more atom-economical but the reactions often require rigorous optimization and can only be done with specific substrates.[71,72] In our group we have optimized a set of DHA conditions that work well for PDI and we chose to begin with these conditions to synthesize our target $(PDI)_2Th_2B$ (Figure 3A).[73] The starting materials $(FMes)BTh_2$ and PDI–Br were reacted until no further change was observed *via* thin layer chromatography (TLC). The crude solid was isolated *via* precipitation from MeOH and analysed by TLC which indicated the presence of two major products. These were separated by column chromatography. Analysis by ^1H NMR spectroscopy indicated that neither of these fractions contained the target compound, nor did they contain any trace of the (FMes)B moiety as indicated by the lack of the singlet 2H peak of the FMes group. However, fractions 1 and 2 were identified as PDI–Th and PDI–Th–PDI (Figure 3A), respectively, which have been previously synthesized *via* other means in our group.[41] The source of these products became clear when we considered that the strongly basic reaction conditions promote activation of the B–C(thienyl) bond of the $(FMes)BTh_2$ starting material. In other words, the reagents underwent Suzuki coupling to produce PDI–Th followed by DHA to produce PDI–Th–PDI (Figure 3B). To verify that this sequential Suzuki + DHA coupling was possible, the reaction was reattempted with identical conditions using 2-thienylboronic acid in place of the

(FMes)BTh_2 (Figure 3C). Once again, a mixture of PDI–Th and PDI–Th–PDI was obtained with PDI–Th–PDI being the major product in a 34% yield. This result confirms sequential cross-coupling is occurring. There is precedence for this type of reactivity and it is of interest to rapidly create new organic π-conjugated molecules.[74]

From these results it was clear that $(PDI)_2Th_2B$ could not be synthesized *via* DHA. In order to obtain the target compound, we turned to Stille coupling.[53,75] The stannylated (FMes)BTh_2 reagent was synthesized following the literature procedure[75] and reacted with PDI–Br using $Pd_2(dba)_3$/P(*o*-tol)$_3$ as the catalyst (Figure 4). The target compound was obtained selectively and isolated as a solid (78% yield). Other palladium catalysts were also screened, but lower yields were obtained from these reactions due to de-borylation and by-product formation. Whereas previous research has focused on boron's incorporation into NFAs as a tetracoordinate borate,[22,27,49] this is the first report on the synthesis of a PDI-based NFA possessing a tricoordinate borane.

The product was characterized by ^1H, ^{11}B, ^{19}F, and ^{13}C NMR spectroscopy, mass spectrometry, and elemental analysis. The ^{11}B NMR spectrum showed a very broad signal at ca. 55 ppm in the region typical of tricoordinate organoboranes and at a similar chemical shift as the precursor (SI, Figure S2), confirming that the borane moiety remained intact. In addition, following previous work,[53] 20 equivalents of tetrabutyl-ammonium fluoride were added to a sample of $(PDI)_2Th_2B$. The product gave a characteristic ^{11}B NMR spectroscopic signal at 3.5 ppm for the expected tetracoordinate borate complex (SI, Figure S3).

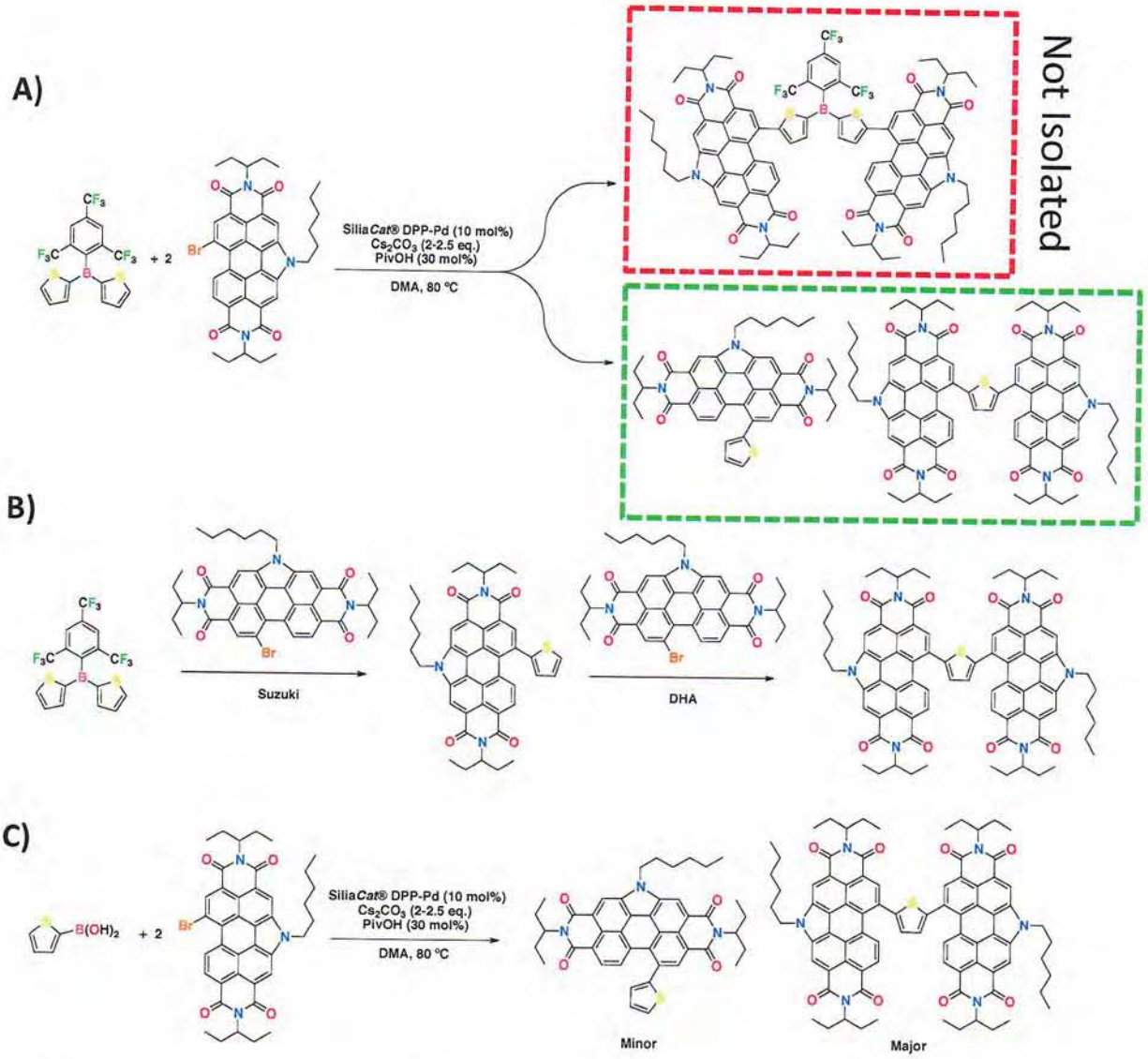

Figure 3: A) The proposed synthesis of the target compound $(PDI)_2Th_2B$ (red box) and the actual products PDI–Th and PDI–Th–PDI (green box). B) The proposed method by which PDI–Th and PDI–Th–PDI were generated. C) The synthesis of PDI–Th and PDI–Th–PDI *via* sequential Suzuki + DHA coupling methods.

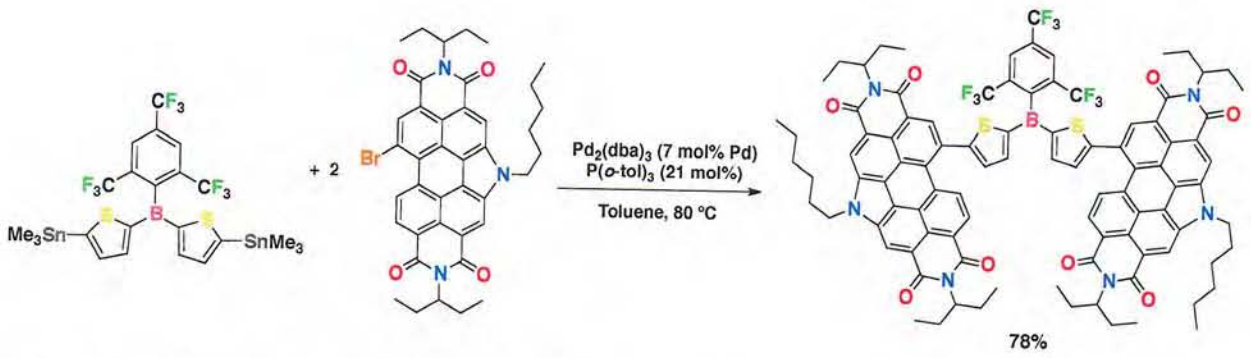

Figure 4: The synthesis of $(PDI)_2Th_2B$ *via* Stille coupling.

2.3. Optoelectronic properties

The electrochemical properties of $(PDI)_2Th_2B$ were measured *via* cyclic voltammetry and differential pulse voltammetry while optical properties determined by UV/Vis absorption and emission spectroscopy. The optoelectronic properties were then compared with those of $(PDI)_2Th_2$ and $(PDI)_2Th_2PO$ to study the influence of the functionalization of the core.[35,41] Our previous work has shown that for PDI–π-core–PDI compounds functionalized with varying π-cores, the LUMO energy level reflects that of the PDI moieties and so remains relatively constant while the HOMO energy level is much more heavily influenced by the π-core.[36–38] This allows the band gap of PDI–π-core–PDI based materials to be tuned through variation of the π-core. Similarly, the optical properties tend to be dominated by the characteristic signatures of the PDI moieties but the absorption can also be enhanced and extended by strongly absorbing π-cores.[37,38] In this work we observe the same effects where modification of the bithiophene core with borane or phosphole has affected the HOMO energy level and optical absorption.

The cyclic voltammogram (referenced to Fc^+/Fc) of $(PDI)_2Th_2B$ is displayed in Figure 5 along with those of $(PDI)_2Th_2$ and $(PDI)_2Th_2PO$. The cyclic voltammograms of all three compounds, obtained in CH_2Cl_2, each show one oxidation wave and two reduction waves, characteristic for PDI-based materials.[41] An additional irreversible reduction wave was also found

for $(PDI)_2Th_2B$ when data were acquired in THF, which has a larger electrochemical window (onset = ca. -2.36 V, SI, Figure S11), which is attributed to reduction at the boron centre. The potential is more cathodic than typically observed for these types of arylboranes[53] due to the accumulation of a large negative charge from the PDI^{2-} units. The oxidation and reduction onset and $E_{1/2}$ potentials, IP, EA, and electrical band gaps (E_g) are displayed in Table 1 for $(PDI)_2Th_2$, $(PDI)_2Th_2PO$, and $(PDI)_2Th_2B$. As expected for PDI–π-core–PDI materials, the three compounds have very similar EAs, particularly $(PDI)_2Th_2PO$ and $(PDI)_2Th_2B$ (ca. 3.62 eV) with $(PDI)_2Th_2$ slightly lower (3.59 eV). As discussed previously, the addition of the phosphole in the bithiophene core stabilizes LUMO energy through overlap of the bithiophene π* orbital and P–Ph σ*.[48] In parallel, overlap of the thiophene π* orbitals and B p_z orbital, as discussed above, results in a similar effect increasing the EA of $(PDI)_2Th_2B$.[26]

Varying the π-core has a much more profound effect on the oxidation potentials of the molecules, as can been seen in Figure 5. With the addition of the phosphoryl and borane units, the IP increases from 5.62 eV in $(PDI)_2Th_2$ to 5.74 eV in $(PDI)_2Th_2PO$ and 5.82 eV in $(PDI)_2Th_2B$, a difference of 0.1 and 0.2 eV, respectively. The increase in IP with P and B addition is again consistent with these heteroatoms removing electron dentistry along the π-conjugated backbone. The changes in IP and EA are reflected in the electrochemical band gaps where $(PDI)_2Th_2$ has the smallest band gap at 2.03 eV, $(PDI)_2Th_2PO$ has a larger band gap at 2.12 eV, and $(PDI)_2Th_2B$ has the largest band gap at 2.20 eV.

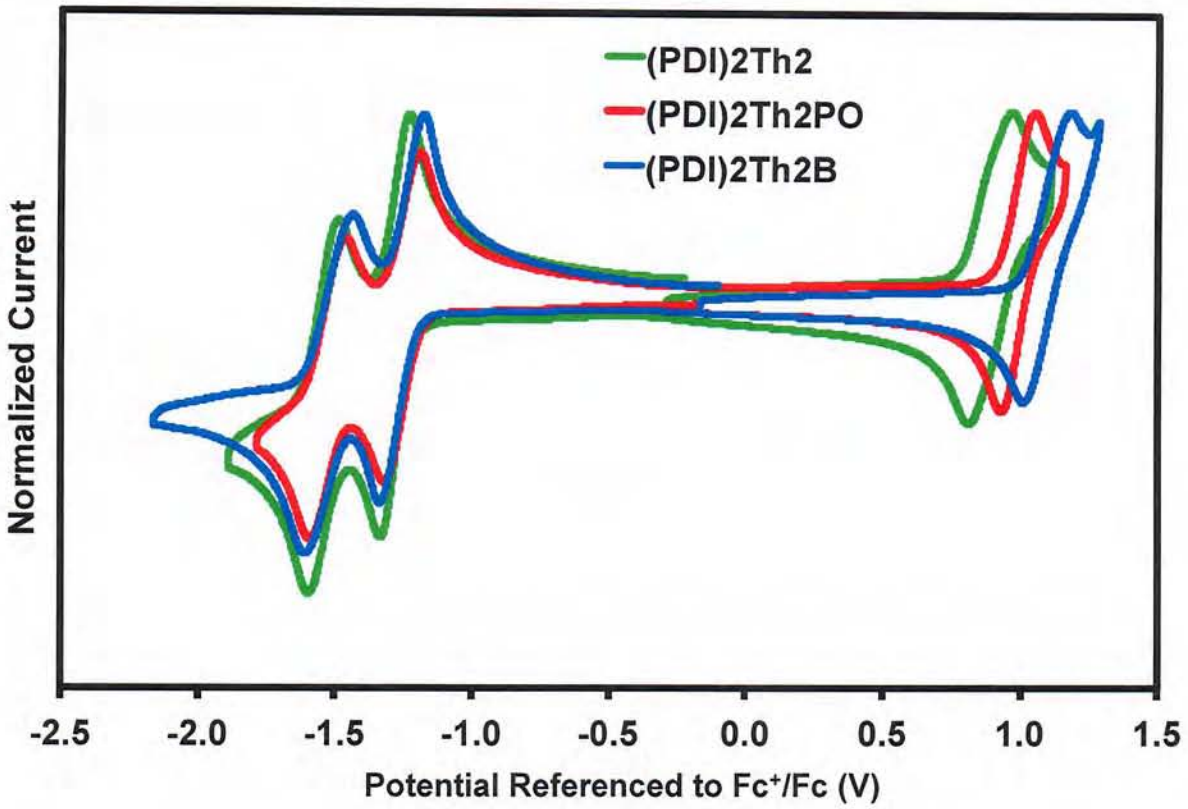

Figure 5: Cyclic voltammograms for $(PDI)_2Th_2$,[41] $(PDI)_2Th_2PO$,[35] and $(PDI)_2Th_2B$ acquired in CH_2Cl_2 solvent at a scan rate of 100 mV/s, normalized to the oxidation maximum.

Table 1: Electrical data for the three acceptor compounds.

	$(PDI)_2Th_2$[41]	**$(PDI)_2Th_2PO$**[35]	**$(PDI)_2Th_2B$**
E_{Onset} Ox (V)	-0.82	-0.94	-1.02
$E_{1/2}$ Ox (V)	-0.93	-1.01	-1.10
E_{Onset} Red (V)	-1.21	-1.18	-1.18
$E_{1/2}$ Red (V)	-1.27, -1.53	-1.26, -1.53	-1.25, -1.52
IP (eV)[a]	-5.62	-5.74	-5.82
EA (eV)[a]	-3.59	-3.62	-3.62
E_g (eV)	-2.03	-2.12	-2.20

[a]Energies were calculated by (E_{Onset}+4.8) where Fc HOMO = 4.8 eV.[76]

UV/Vis absorption and emission profiles of the three compounds in the solution and solid-states are displayed in Figure 6. The absorption and emission maxima, Stokes shifts, and optical band gaps are displayed in Table 2. The absorption profiles of each compound in solution are shown in Figure 6A. All are dominated by the PDI chromophore with characteristic vibrionic peaks at 535 nm (0-0 transition) and 490 nm (0-1 transition). $(PDI)_2Th_2$ and $(PDI)_2Th_2PO$ have identical ratios between the 0-0 and 0-1 peaks while $(PDI)_2Th_2B$ has a lower intensity of the 0-1 peak compared to its 0-0 peak. This difference is a result of the B moiety influencing the electronics of the molecule by isolating the PDI–Th units. Essentially, absorption in $(PDI)_2Th_2B$ is from isolated PDI–Th units, whereas absorption in $(PDI)_2Th_2$ and $(PDI)_2Th_2PO$ occurs over a larger PDI–Th–Th–PDI system, resulting in the slightly different profiles. This is shown by the similar absorption profiles of $(PDI)_2Th_2B$ and pure PDI–Th (SI, Figure S17). At the higher energy portion of the spectrum the profiles differ according to the cores of each compound, with $(PDI)_2Th_2PO$ absorbing at lower energy (ca. 450–350 nm) than $(PDI)_2Th_2$ and $(PDI)_2Th_2B$ (each absorbing from 400 nm). This is in agreement with the previously reported absorption profiles for each bithiophene core.[52,77,78] The molar extinction coefficients (ε) are largely consistent between $(PDI)_2Th_2$ and $(PDI)_2Th_2PO$ (93 000 $Lmol^{-1}cm^{-1}$ and 90 000 $Lmol^{-1}cm^{-1}$, respectively), but the addition of boron results in a significantly larger ε of 132 000 $Lmol^{-1}cm^{-1}$. This is likely due to the influence of the B moiety on the electronics. As mentioned previously, the borane enables ICT between the B p_z orbital the π system of the substituents.[26] This has been shown to increase optical absorption in a number compounds possessing triaryl borane moieties.[79–82] Another possibility is the influence of the borane on the geometry. Given how DFT calculations show that $(PDI)_2Th_2B$ possesses a much

higher degree of twist, it is possible that this enables a higher area of absorption in the molecular architecture compared to the more constrained $(PDI)_2Th_2$ and $(PDI)_2Th_2PO$.

The film absorption profiles (Figure 6B) are all very similar, showing a slight red-shift in peak maxima and a broadening of the profiles. The 0-0 to 0-1 peak ratios have all increased as well compared to their solution counterparts with the three compounds becoming more like each other, which is indicative of the geometric differences between the compounds becoming less pronounced in the solid state.

In solution, the $(PDI)_2Th_2$ has the lowest energy emission maximum at 667 nm. Functionalizing the bithiophene core with a phosphoryl group blue-shifts the emission maximum to 638 nm while functionalizing with boron blue-shifts the emission maximum further to 588 nm. In the solid-state, both $(PDI)_2Th_2$ and $(PDI)_2Th_2PO$ have very similar emission maxima at 698 nm and 692 nm, respectively, while the $(PDI)_2Th_2B$ emission maximum is blue-shifted to 631 nm. The large blue-shift in emission of $(PDI)_2Th_2B$ compared to $(PDI)_2Th_2$ and $(PDI)_2Th_2PO$ is possibly due to the boron moiety isolating the PDI–Th units of the compound, as was indicated by the DFT calculations above. Charge transfer in $(PDI)_2Th_2$ and $(PDI)_2Th_2PO$ is likely more pronounced due to those species possessing a bithiophene moiety, leading to lower energy emission maxima. In $(PDI)_2Th_2B$ the splitting of the bithiophene moiety with B and increased conformational disorder may localize the electronic transition to the PDI–Th, giving higher energy emission. To test this hypothesis, the emission in solution of $(PDI)_2Th_2B$ was compared to the emission of a pure sample of PDI–Th. Their emission profiles were identical (SI, Figure S17), supporting the theory that localized PDI–Th emission in $(PDI)_2Th_2B$ is responsible for its higher energy emission maximum. The quantum yield for $(PDI)_2Th_2B$ was also measured and found to be 61%, compared to 97% for $(PDI)_2Th_2PO$, indicating some energy loss to non-radiative pathways, which once again is likely due to the higher rotational degrees of freedom in $(PDI)_2Th_2B$

than in $(PDI)_2Th_2PO$. The optical band gaps were calculated from the intercept of absorption and emission (solution and solid-state). They follow a similar trend as that observed for the electrical band gaps, where $(PDI)_2Th_2$ and $(PDI)_2Th_2PO$ are similar while $(PDI)_2Th_2B$ is the largest. All this data shows how π-core functionalization can be an effective means of tuning the optical properties in the PDI–π-core–PDI framework, making this a versatile framework for organic materials.

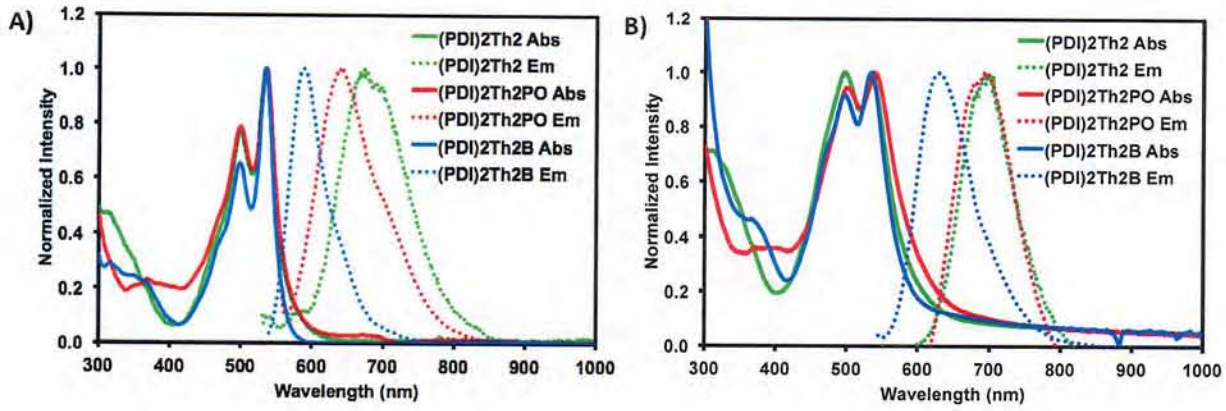

Figure 6: Absorption and emission profiles for $(PDI)_2Th_2$,[41] $(PDI)_2Th_2PO$,[35] and $(PDI)_2Th_2B$ in A) $CHCl_3$ solution and B) solid-state, spun-cast from 10 mg/mL $CHCl_3$ solutions.

Table 2: Optical data for the three acceptor compounds.

	$(PDI)_2Th_2$[41]	**$(PDI)_2Th_2PO$**[35]	**$(PDI)_2Th_2B$**
Soln Abs λ_{max} (nm)	533	536	534
Soln Em λ_{max} (nm)	667	638	588
Soln E_g (eV)[a]	2.14	2.16	2.23
Soln Stokes Shift (eV)[b]	0.48	0.37	0.21
ε (L mol^{-1} cm^{-1})	93 000	90 000	132 000
Film Abs λ_{max} (nm)	535	538	534

Film Em λ_{max} (nm)	698	692	631
Film E_g (eV)[a]	1.97	1.96	2.13
Film Stokes Shift (eV)[b]	0.53	0.51	0.36

[a]Optical band gaps were calculated from the wavelength intercept of abs and em profiles where ($E_{\lambda int} = h*c/\lambda_{int}$; h = Planck's Constant, c = speed of light). [b]Stokes Shifts were calculated by ($E_{\lambda abs} - E_{\lambda ems}$) where ($E_{\lambda max} = h*c/\lambda_{max}$).

2.4. Thermal properties

The thermal properties were investigated by differential scanning calorimetry (DSC) and thermal gravimetric analysis (TGA). The DSC and TGA results are displayed in Figure 7. The $(PDI)_2Th_2$ shows no indication of a melt or crystallization between 50 °C and 350 °C while $(PDI)_2Th_2PO$ shows a melt at 278 °C and crystallization at 233 °C. The $(PDI)_2Th_2B$ only shows a melt or glass transition at 239 °C. The lower melting temperature of $(PDI)_2Th_2B$ compared to $(PDI)_2Th_2PO$ is likely due to the increased rotational freedom of $(PDI)_2Th_2B$ leading to weaker intermolecular forces. The $(PDI)_2Th_2$ is the most thermally stable, decomposing at 427 °C. Functionalizing the bithiophene core slightly reduces the thermal stability with $(PDI)_2Th_2PO$ decomposing at 415 °C and $(PDI)_2Th_2B$ decomposing at 396 °C. This is likely due to the lower stability of the C–P and C–B bonds, respectively. The TGA profile for $(PDI)_2Th_2B$ also shows a greater mass percentage loss than the other two compounds, implying a greater fraction of the molecule breaking apart. In $(PDI)_2Th_2$ and $(PDI)_2Th_2PO$ the mass percentage decrease roughly corresponds to the loss of the alkyl chains from the PDI units, while in $(PDI)_2Th_2B$ the larger decrease corresponds to the loss of the FMes unit in addition to the alkyl chains. However, the thermal stability of $(PDI)_2Th_2B$ is consistent with TGA analysis on polymers of $(FMes)BTh_2$, which were stable up to 300 °C.[75]

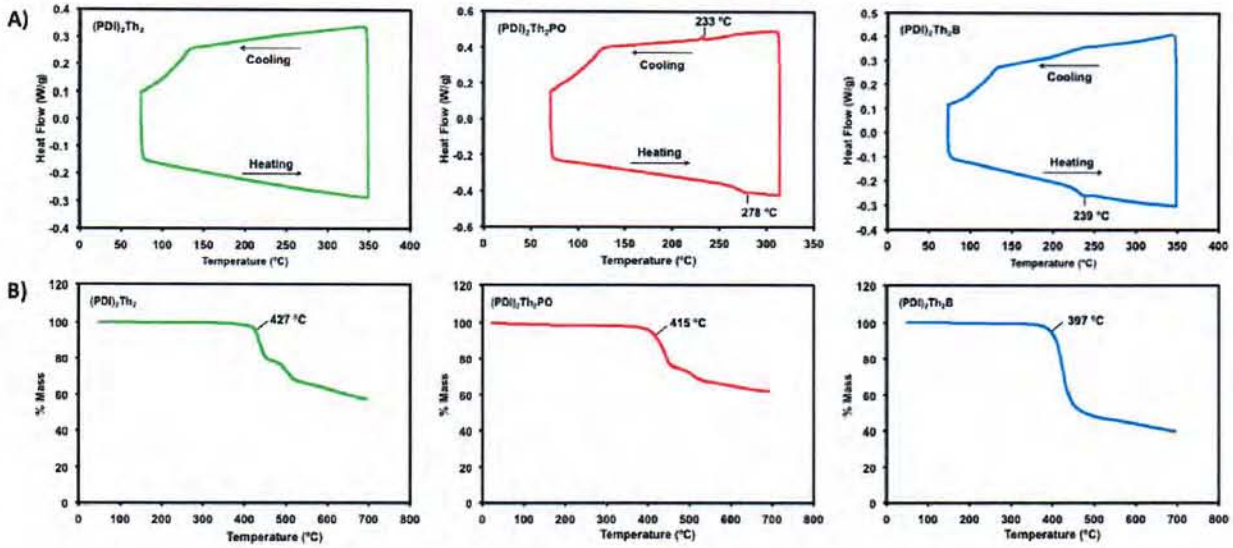

Figure 7: A) DSC profiles and B) TGA profiles for $(PDI)_2Th_2$, $(PDI)_2Th_2PO$,[35] and $(PDI)_2Th_2B$.

2.5. Photovoltaic device fabrication

The PDI–π-core–PDI framework has proven to be effective as a non-fullerene acceptor (NFA) in organic BHJ solar cells.[30,36,38] Both $(PDI)_2Th_2$ and $(PDI)_2Th_2PO$ have been used as NFAs with the donor polymer PTB7-Th with moderate results.[35,41] We have recently demonstrated that the quinoxaline-based polymer TTFQx-T1[83] (Figure 8A, also referred to as QX-1 by our teams) is a good match for PDI NFAs and was chosen for this study.[84,85] Casting active layers of donor polymer/small molecule acceptor blends often requires the use of chlorinated solvents such as chloroform or *o*-dichlorobenzene. These solvents tend to be more toxic than non-chlorinated solvents and wreak havoc on the upper atmosphere,[86,87] which hinders the overall long term environmental sustainability of such systems. We therefore fabricated all active layers using the eco-friendly solvent 2-methyltetrahydrofuran (2Me-THF). Furthermore, because a certain degree of phase separation in the BHJ layer is necessary to promote charge separation and conductivity,[88] it is often necessary to use thermal annealing,[89] solvent vapour annealing,[90] or solvent additives.[2]

These processing techniques can induce molecular reorganization leading to greater phase separation and domain purity through aggregation, improving performance.[91,92] Our previous work has shown that PDI–π-core–PDI acceptors tend to re-organize in the film to form more ordered nanostructures upon exposure to solvent vapours either through solvent vapour annealing[29,30] or through solvent additives.[36] For TTFQx-T1 it is known that thermal annealing at temperatures above 180 °C crystallizes the polymer leading to improved BHJs for better OSC performance. Thus, for this study we evaluated OSC devices with active layers of TTFQx-T1 and the three acceptor compounds processed from 2-MeTHF and processed using thermal annealing with and without the solvent additive diphenyl ether (DPE).

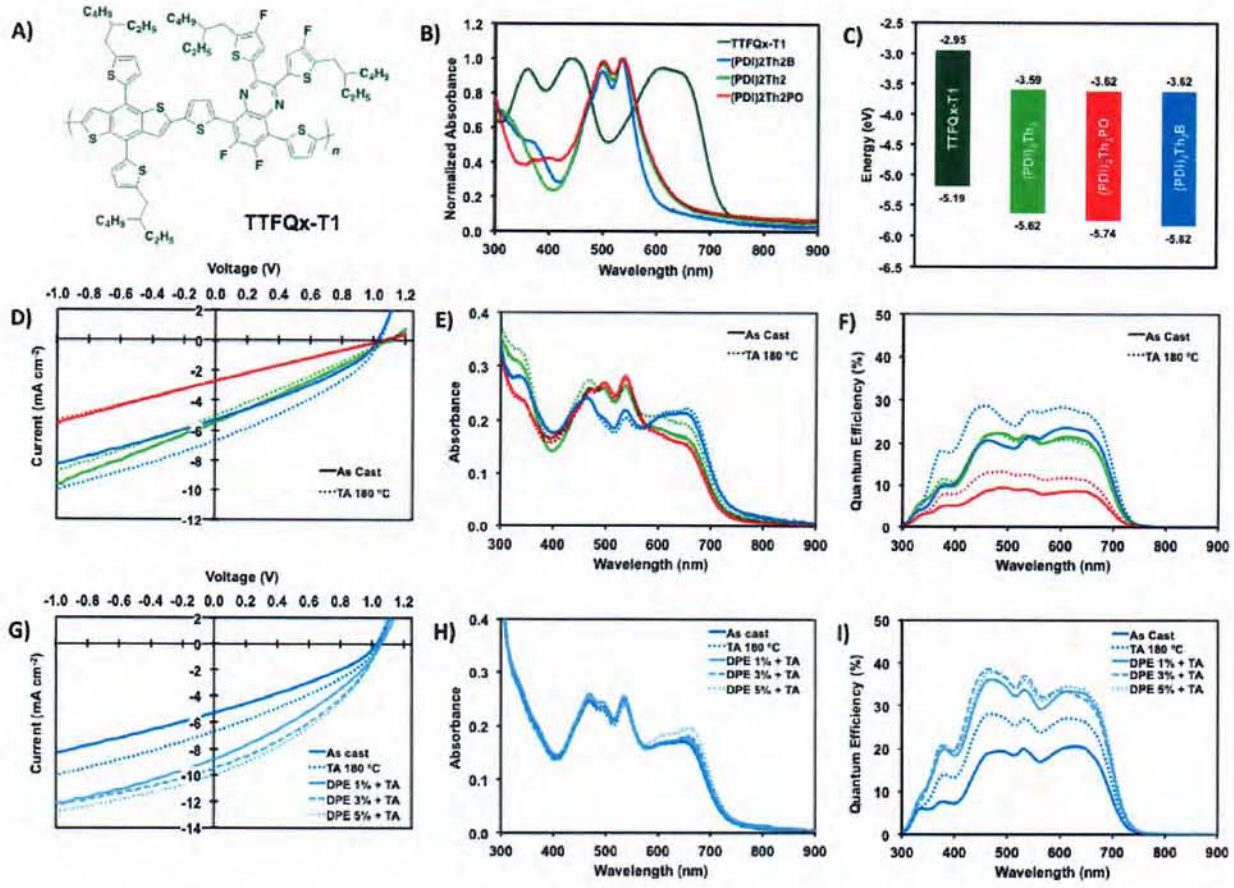

Figure 8: A) Donor polymer TTFQx-T1. B) Normalized thin film absorption profiles for active layer materials cast from 2-MeTHF. C) Energy level diagram for active layer materials determined

by CV. D) *JV* curves, E) absorption profiles, and F) external quantum efficiency for best devices as cast and thermally annealed of 50:50 TTFQx-T1/acceptor compounds blends. G) *JV* curves, H) absorption profiles, and I) external quantum efficiency for best devices as thermally annealed and with DPE additive of 50:50 TTFQx-T1/$(PDI)_2Th_2B$ blends.

Table 3: Summary of optimized organic solar cell data.[a]

Materials	Processing[b]	V_{oc} (V)	J_{sc} (mA/cm^2)	FF (%)	PCE (%)
		Avg. (best)	Avg. (best)	Avg. (best)	Avg. (best)
TTFQx-T1/$(PDI)_2Th_2$	As cast	1.10 (1.09)	5.25 (5.43)	26.9 (27.1)	1.55 (1.61)
TTFQx-T1/$(PDI)_2Th_2PO$	As cast	1.03 (1.07)	2.72 (2.29)	24.7 (24.5)	0.59 (0.71)
TTFQx-T1/$(PDI)_2Th_2B$	As cast	1.01 (1.01)	5.11 (5.30)	32.8 (33.0)	1.69 (1.77)
TTFQx-T1/$(PDI)_2Th_2$	TA	1.12 (1.13)	5.26 (5.54)	25.9 (25.5)	1.52 (1.59)
TTFQx-T1/$(PDI)_2Th_2PO$	TA	1.05 (1.05)	2.69 (2.70)	25.0 (25.4)	0.70 (0.71)
TTFQx-T1/$(PDI)_2Th_2B$	TA	1.03 (1.03)	6.72 (6.93)	33.2 (32.5)	2.29 (2.33)
TTFQx-T1/$(PDI)_2Th_2B$	DPE 1%; TA	1.05 (1.05)	8.47 (8.81)	33.4 (33.3)	2.96 (3.08)
TTFQx-T1/$(PDI)_2Th_2B$	DPE 3%; TA	1.04 (1.04)	9.45 (9.51)	36.6 (36.7)	3.60 (3.64)
TTFQx-T1/$(PDI)_2Th_2B$	DPE 5%; TA	1.03 (1.03)	9.32 (10.00)	36.7 (37.3)	3.52 (3.85)

[a]Device architecture: ITO/ZnO/BHJ/MoO_x/Ag. Active layers were spin cast at 1500 rpm from 10 mg/mL solutions in 2-MeTHF of 50:50 TTFQx-T1/acceptor ratios.

[b]TA = thermal annealing 180 °C, 10 min; DPE = diphenyl ether solvent additive.

OSCs were fabricated based on our prior work[30,93] using an air-processed and air-tested protocol with an inverted framework: ITO/ZnO/BHJ/MoO_x/Ag.[94] Active layers of TTFQx-T1/acceptor (50:50) were cast at 1500 rpm for 60 seconds from 1 wt/v% solutions in 2-MeTHF. They were subject to thermal annealing at 180 °C for 10 min after being left to dry for 12 hours prior to electrode deposition. Complete results are available in the SI and summarized in Table 3.

Figure 8D/E/F displays the *JV* curves, absorption profiles, and EQE profiles, respectively, for the best devices under each condition. All blends showed partial quenching of the polymer emission in both as cast and thermally annealed films (SI, Figure S19).

Previously, $(PDI)_2Th_2$ and $(PDI)_2Th_2PO$ have been paired with PTB7-Th to give optimum performances with average PCEs of 2.6% and 1.9%, respectively.[35,41] This study represents the first pairing of these compounds with TTFQx-T1 and the first use of $(PDI)_2Th_2B$ in OSC devices. As can be seen in Table 3 and Figure 8D, all devices had high V_{OC} >1 V. However, for $(PDI)_2Th_2$ and $(PDI)_2Th_2PO$, J_{sc} and FF were low leading to low PCEs for both as cast and thermally annealed devices. The *JV* curves and EQE profiles for $(PDI)_2Th_2$ and $(PDI)_2Th_2PO$ blends show little difference between as-cast and thermally annealed devices (Figure 8D/F). However, with $(PDI)_2Th_2B$, an increase in performance was observed from a PCE of 1.69% to 2.29% upon thermal annealing, which was also reflected by improvement in the *JV* curve and EQE profile. Atomic force microscopy (AFM) images were taken of the best devices under each condition and are shown in Figure 9. AFM phase images are available in the SI. All films showed similar fibrillar morphologies but the TTFQx-T1/$(PDI)_2Th_2B$ film, thermally annealed, did show an increase in the roughness from the untreated "as-cast" film as well as slightly more definition to the domains. This may be an indication of the individual polymer or NFA becoming more ordered within their respective domains. To improve PCE, we envisioned increasing phase separation *via* solvent treatment followed by thermal annealing to increase order within domains.

Solvent vapours have been shown to be an effective way of inducing phase separation in the active layer.[95] A high boiling point solvent added to the ink solution is presumed, upon casting, to remain in the film allowing for slow evaporation which ideally modifies the morphology to a more ordered state.[96] There are many high boiling point solvents to choose but to maintain the theme of green processing conditions for this study we chose to use DPE, a non-halogenated, high

boiling (259 °C) solvent.[97,98] DPE was added in 1, 3, and 5% v/v concentrations to ink solutions of $(PDI)_2Th_2B$ and TTFQx-T1, still keeping with the 1 wt/v% concentration in 2Me-THF and 50:50 ratio. Upon casting the films were left for 24 hours to allow for slow evaporation. They were then thermally annealed at 180 °C for 10 min. The results are summarized in Table 3. Figure 8G/H/J displays the *JV* curves, absorption profiles, and EQE profiles, respectively, for the best devices under each condition along with the previous results for TTFQx-T1/$(PDI)_2Th_2B$ blends. Complete results are in the SI.

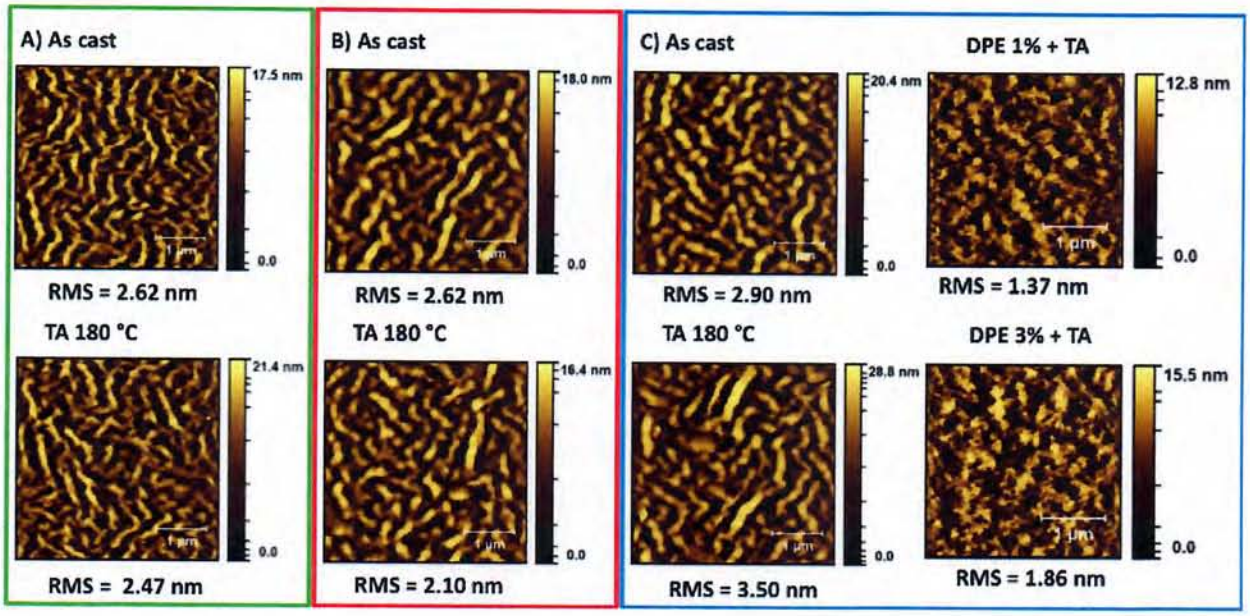

Figure 9: AFM images for A) TTFQx-T1/$(PDI)_2Th_2$, B) TTFQx-T1/$(PDI)_2Th_2PO$, and C) TTFQx-T1/$(PDI)_2Th_2B$ blends with processing conditions shown.

For TTFQx-T1/$(PDI)_2Th_2B$ devices treated with DPE and thermally annealed, V_{OC} remained high at >1 V while J_{sc}, FF, and PCE all increased for all three DPE concentrations. Despite the improvement, FF remained below 40%, which is typical for our previous N-annulated PDI-based materials.[35,36,41,88] The EQE also increased across the spectrum for all DPE concentrations with 3% and 5% giving the highest values. The best device was obtained with 5%

DPE concentration giving a PCE of 3.85%. However, the 3% DPE concentration gave more consistent results with an average PCE of 3.60% compared to 3.52% average for 5% DPE. From the AFM images, displayed in Figure 9, the DPE treated films are much less fibrillar than the previous TTFQx-T1/$(PDI)_2Th_2B$ films and the roughness has decreased. While the 1% DPE treated film still retains some semblance of the fibrillar morphology, the 3% DPE treated film shows domains that appear more evenly distributed. The 5% DPE treated film had identical morphology to the 3% DPE treated film with increased roughness (SI, Figure S22). This indicates the additive has had a significant impact on the film morphology and the increased performance is due to more favourably distributed and purer domains leading to enhanced charge separation.

Once again, this is the first demonstration of a PDI-based NFA with tricoordinate borane moiety. Unlike previous examples of boron-based NFAs which involved tetracoordinate borate to constrain the geometry, [22,27] this research presents an example of a tricoordinate borane providing more flexibility to the acceptor enabling it to adopt a more favoured solid state morphology in the BHJ layer.

3. Conclusions

We have reported on the synthesis of a new boron based non-fullerene acceptor for energy application. The new material has a borane-functionalized bithiophene core with PDI end caps, $(PDI)_2Th_2B$. The synthesis was attempted *via* DHA methods but, due to the reactive boron centre, the substrate underwent sequential Suzuki/DHA coupling to give PDI–Th–PDI. The target compound $(PDI)_2Th_2B$ was successfully synthesized *via* Stille coupling in a 78% yield. It was fully characterized and compared with phosphoryl-functionalized $(PDI)_2Th_2PO$ and unfunctionalized $(PDI)_2Th_2$ materials to highlight the differences in optical properties and electronic energy levels.

Density functional theory calculations showed that the boron-substituted compound had a much larger degree of twist than the fused phosphole and unfunctionalized compounds, disrupting the conjugation across the whole molecular scaffold. All three compounds had similar optoelectronic properties though $(PDI)_2Th_2B$ did have a larger band gap and blue-shifted emission compared to $(PDI)_2Th_2$ and $(PDI)_2Th_2PO$, which was attributed to the influence of the boron atom on the molecular electronics and geometry.

As a proof of concept, the three compounds were paired with the donor polymer TTFQx-T1 and solar cell devices were fabricated using exclusively green processing conditions. Solar cells were fabricated in air while active layers were solution processed from the eco-friendly solvent 2Me-THF (with or without the volatile solvent additive diphenyl ether) under ambient conditions. The TTFQx-T1/$(PDI)_2Th_2B$ blend was consistently higher performing than the TTFQx-T1/$(PDI)_2Th_2$ and TTFQx-T1/$(PDI)_2Th_2PO$ blends. All organic solar cells had high open circuit voltages above 1 V, but those using the TTFQx-T1/$(PDI)_2Th_2B$ active layer exhibited high short-circuit currents leading to the better performance. A maximum PCE of 3.6% was achieved after active layer optimization using solvent additives.

This is the first report on a PDI-based borane-functionalized molecular non-fullerene acceptor. We speculate that the greater flexibility afforded by the borane unit allowed for a more favourable active layer morphology with $(PDI)_2Th_2B$ and the polymer. This is in contrast to previous example of boron-based NFAs, which used tetracoordinate borate units to constrain and planarize the geometry. Our results are consistent with recent literature that shows PDI materials that adopt a more isotropic shape are better non-fullerene acceptors than those with planar structures.

These results support the small yet growing body of literature that demonstrate the potential of organo-main group element functional groups to be used to fabricate new and relevant organic semiconducting materials for energy applications.

4. Conflicts of interest

There are no conflicts to declare.

5. Acknowledgements and Funding Sources

GCW acknowledges NSERC DG (435715-2013) and CFI JELF (34102). GCW and TB acknowledge the Canadian Research Chairs Program. TAW is grateful for a University of Calgary Eyes High post-graduate scholarship. AL acknowledges NSERC for a postdoctoral fellowship. This research was undertaken thanks in part to funding from the Canada First Research Excellence Fund (CFREF). All authors are thankful to the University of Calgary and Rutgers University for research infrastructure support. Drs Xiaodong Yin (USA, Rutgers) and Yingping Zou (China, CSU) are thanked for supplying a part of the bis(thien-2-yl)(2,4,6-tris(trifluoromethyl)phenyl) borane and the TTFQx-T1 polymer samples, respectively. FJ and AFA thank the US National Science Foundation (NSF) for support under grant CHE-1664975.

6. Notes and Reference

(1) Forrest, S. R. The Path to Ubiquitous and Low-Cost Organic Electronic Appliances on Plastic. *Nature* **2004**, *428* (6986), 911–918.

(2) Sun, Y.; Welch, G. C.; Leong, W. L.; Takacs, C. J.; Bazan, G. C.; Heeger, A. J. Solution-Processed Small-Molecule Solar Cells with 6.7% Efficiency. *Nat. Mater.* **2012**, *11* (1), 44–48.

(3) Zhang, Q.; Kan, B.; Liu, F.; Long, G.; Wan, X.; Chen, X.; Zuo, Y.; Ni, W.; Zhang, H.; Li, M.; et al. Small-Molecule Solar Cells with Efficiency over 9%. *Nat. Photonics* **2015**, *9* (1), 35–41.

(4) Liu, J.; Chen, S.; Qian, D.; Gautam, B.; Yang, G.; Zhao, J.; Bergqvist, J.; Zhang, F.; Ma, W.; Ade, H.; et al. Fast Charge Separation in a Non-Fullerene Organic Solar Cell with a Small Driving Force. *Nat. Energy* **2016**, *1* (7), 16089.
(5) Hou, J.; Inganäs, O.; Friend, R. H.; Gao, F. Organic Solar Cells Based on Non-Fullerene Acceptors. *Nat. Mater.* **2018**, *17* (2), 119–128.
(6) Facchetti, A. π-Conjugated Polymers for Organic Electronics and Photovoltaic Cell Applications. *Chem. Mater.* **2011**, *23* (3), 733–758.
(7) Mei, J.; Diao, Y.; Appleton, A. L.; Fang, L.; Bao, Z. Integrated Materials Design of Organic Semiconductors for Field-Effect Transistors. *J. Am. Chem. Soc.* **2013**, *135* (18), 6724–6746.
(8) Sirringhaus, H. 25th Anniversary Article: Organic Field-Effect Transistors: The Path Beyond Amorphous Silicon. *Adv. Mater.* **2014**, *26* (9), 1319–1335.
(9) Gather, M. C.; Köhnen, A.; Meerholz, K. White Organic Light-Emitting Diodes. *Adv. Mater.* **2011**, *23* (2), 233–248.
(10) Xiao, L.; Chen, Z.; Qu, B.; Luo, J.; Kong, S.; Gong, Q.; Kido, J. Recent Progresses on Materials for Electrophosphorescent Organic Light-Emitting Devices. *Adv. Mater.* **2011**, *23* (8), 926–952.
(11) Xu, R.-P.; Li, Y.-Q.; Tang, J.-X. Recent Advances in Flexible Organic Light-Emitting Diodes. *J. Mater. Chem. C* **2016**, *4* (39), 9116–9142.
(12) Yamaguchi, S.; Wakamiya, A. Boron as a Key Component for New π-Electron Materials. *Pure Appl. Chem.* **2006**, *78* (7), 1413–1424.
(13) Wakamiya, A.; Taniguchi, T.; Yamaguchi, S. Intramolecular B–N Coordination as a Scaffold for Electron-Transporting Materials: Synthesis and Properties of Boryl-Substituted Thienylthiazoles. *Angew. Chem. Int. Ed.* **2006**, *45* (19), 3170–3173.
(14) Jäkle, F. Lewis Acidic Organoboron Polymers. *Coord. Chem. Rev.* **2006**, *250* (9), 1107–1121.
(15) Jäkle, F. Advances in the Synthesis of Organoborane Polymers for Optical, Electronic, and Sensory Applications. *Chem. Rev.* **2010**, *110* (7), 3985–4022.
(16) Haiyan Li; Anand Sundararaman; Krishnan Venkatasubbaiah, and; Jäkle*, F. Organoborane Acceptor-Substituted Polythiophene via Side-Group Borylation https://pubs.acs.org/doi/full/10.1021/ja068771b (accessed Dec 3, 2018).
(17) Li, H.; Jäkle, F. Donor–π–Acceptor Polymer with Alternating Triarylborane and Triphenylamine Moieties. *Macromol. Rapid Commun.* **2010**, *31* (9–10), 915–920.
(18) Yamaguchi, S.; Akiyama, S.; Tamao, K. Colorimetric Fluoride Ion Sensing by Boron-Containing π-Electron Systems. *J. Am. Chem. Soc.* **2001**, *123* (46), 11372–11375.
(19) Yamaguchi, S.; Akiyama, S.; Tamao, K. A New Approach to Photophysical Properties Control of Main Group Element π-Electron Compounds Based on the Coordination Number Change. *J. Organomet. Chem.* **2002**, *652* (1–2), 3–9.
(20) Wade, C. R.; Broomsgrove, A. E. J.; Aldridge, S.; Gabbaï, F. P. Fluoride Ion Complexation and Sensing Using Organoboron Compounds. *Chem. Rev.* **2010**, *110* (7), 3958–3984.
(21) Rostami, A.; Taylor, M. S. Polymers for Anion Recognition and Sensing. *Macromol. Rapid Commun.* **2012**, *33* (1), 21–34.
(22) Zhao, R.; Dou, C.; Xie, Z.; Liu, J.; Wang, L. Polymer Acceptor Based on B←N Units with Enhanced Electron Mobility for Efficient All-Polymer Solar Cells. *Angew. Chem. Int. Ed.* **2016**, *55* (17), 5313–5317.
(23) Welch, G. C.; Bazan, G. C. Lewis Acid Adducts of Narrow Band Gap Conjugated Polymers. *J. Am. Chem. Soc.* **2011**, *133* (12), 4632–4644.

(24) Welch, G. C.; Coffin, R.; Peet, J.; Bazan, G. C. Band Gap Control in Conjugated Oligomers via Lewis Acids. *J. Am. Chem. Soc.* **2009**, *131* (31), 10802–10803.
(25) *Main Group Strategies towards Functional Hybrid Materials*; Baumgartner, T., Jäkle, F., Eds.; Wiley-VCH: Weinheim, 2018.
(26) Ren, Y.; Jäkle, F. Merging Thiophene with Boron: New Building Blocks for Conjugated Materials. *Dalton Trans.* **2016**, *45* (36), 13996–14007.
(27) Long, X.; Ding, Z.; Dou, C.; Zhang, J.; Liu, J.; Wang, L. Polymer Acceptor Based on Double B←N Bridged Bipyridine (BNBP) Unit for High-Efficiency All-Polymer Solar Cells. *Adv. Mater.* **2016**, *28* (30), 6504–6508.
(28) Min, Y.; Dou, C.; Tian, H.; Geng, Y.; Liu, J.; Wang, L. N-Type Azaacenes Containing B←N Units. *Angew. Chem. Int. Ed.* **2018**, *57* (7), 2000–2004.
(29) McAfee, S. M.; Payne, A.-J.; Dayneko, S. V.; Kini, G. P.; Song, C. E.; Lee, J.-C.; Welch, G. C. A Non-Fullerene Acceptor with a Diagnostic Morphological Handle for Streamlined Screening of Donor Materials in Organic Solar Cells. *J. Mater. Chem. A* **2017**, *5* (32), 16907–16913.
(30) McAfee, S. M.; Dayneko, S. V.; Josse, P.; Blanchard, P.; Cabanetos, C.; Welch, G. C. Simply Complex: The Efficient Synthesis of an Intricate Molecular Acceptor for High-Performance Air-Processed and Air-Tested Fullerene-Free Organic Solar Cells. *Chem. Mater.* **2017**, *29* (3), 1309–1314.
(31) Meng, B.; Ren, Y.; Liu, J.; Jäkle, F.; Wang, L. P–π Conjugated Polymers Based on Stable Triarylborane with n-Type Behavior in Optoelectronic Devices. *Angew. Chem. Int. Ed.* **2018**, *57* (8), 2183–2187.
(32) Langhals, H.; Kirner, S. Novel Fluorescent Dyes by the Extension of the Core of Perylenetetracarboxylic Bisimides. *Eur. J. Org. Chem.* **2000**, *2000* (2), 365–380.
(33) Dayneko, S. V.; Hendsbee, A. D.; Welch, G. C. Combining Facile Synthetic Methods with Greener Processing for Efficient Polymer-Perylene Diimide Based Organic Solar Cells. *Small Methods 2* (6), 1800081.
(34) Payne, A.-J.; Song, J.; Sun, Y.; C. Welch, G. A Tetrameric Perylene Diimide Non-Fullerene Acceptor via Unprecedented Direct (Hetero)Arylation Cross-Coupling Reactions. *Chem. Commun.* **2018**, *54* (81), 11443–11446.
(35) Welsh, T. A.; Laventure, A.; Baumgartner, T.; Welch, G. C. Dithienophosphole-Based Molecular Electron Acceptors Constructed Using Direct (Hetero)Arylation Cross-Coupling Methods. *J. Mater. Chem. C* **2018**, *6* (8), 2148–2154.
(36) Welsh, T. A.; Laventure, A.; Welch, G. C. Direct (Hetero)Arylation for the Synthesis of Molecular Materials: Coupling Thieno[3,4-c]Pyrrole-4,6-Dione with Perylene Diimide to Yield Novel Non-Fullerene Acceptors for Organic Solar Cells. *Molecules* **2018**, *23* (4), 931.
(37) Payne, A.-J.; McAfee, S. M.; Welch, G. C. Optoelectronic Engineering with Organic Dyes: Utilizing Squaraine and Perylene Diimide to Access an Electron-Deficient Molecule with near-IR Absorption. *Chem. Pap.* **2017**, 1–6.
(38) McAfee, S. M.; Dayneko, S. V.; Hendsbee, A. D.; Josse, P.; Blanchard, P.; Cabanetos, C.; Welch, G. C. Applying Direct Heteroarylation Synthesis to Evaluate Organic Dyes as the Core Component in PDI-Based Molecular Materials for Fullerene-Free Organic Solar Cells. *J. Mater. Chem. A* **2017**, *5* (23), 11623–11633.
(39) Zhang, J.; Li, Y.; Huang, J.; Hu, H.; Zhang, G.; Ma, T.; Chow, P. C. Y.; Ade, H.; Pan, D.; Yan, H. Ring-Fusion of Perylene Diimide Acceptor Enabling Efficient Nonfullerene Organic Solar Cells with a Small Voltage Loss. *J. Am. Chem. Soc.* **2017**, *139* (45), 16092–16095.

(40) Luo, Z.; Liu, T.; Cheng, W.; Wu, K.; Xie, D.; Huo, L.; Sun, Y.; Yang, C. A Three-Dimensional Thiophene-Annulated Perylene Bisimide as a Fullerene-Free Acceptor for a High Performance Polymer Solar Cell with the Highest PCE of 8.28% and a VOC over 1.0 V. *J. Mater. Chem. C* **2018**, *6* (5), 1136–1142.
(41) Hendsbee, A. D.; Dayneko, S. V.; Pells, J. A.; Cann, J. R.; Welch, G. C. N-Annulated Perylene Diimide Dimers: The Effect of Thiophene Bridges on Physical, Electronic, Optical, and Photovoltaic Properties. *Sustain. Energy Fuels* **2017**, *1* (5), 1137–1147.
(42) Cann, J.; Dayneko, S.; Sun, J.-P.; Hendsbee, A. D.; Hill, I. G.; Welch, G. C. N-Annulated Perylene Diimide Dimers: Acetylene Linkers as a Strategy for Controlling Structural Conformation and the Impact on Physical, Electronic, Optical and Photovoltaic Properties. *J. Mater. Chem. C* **2017**, *5* (8), 2074–2083.
(43) Baumgartner, T.; Neumann, T.; Wirges, B. The Dithieno[3,2-b:2′,3′-d]Phosphole System: A Novel Building Block for Highly Luminescent π-Conjugated Materials. *Angew. Chem. Int. Ed.* **2004**, *43* (45), 6197–6201.
(44) Hay, C.; Hissler, M.; Fischmeister, C.; Rault-Berthelot, J.; Toupet, L.; Nyulászi, L.; Réau, R. Phosphole-Containing π-Conjugated Systems: From Model Molecules to Polymer Films on Electrodes. *Chem. – Eur. J.* **2001**, *7* (19), 4222–4236.
(45) Hay, C.; Fischmeister, C.; Hissler, M.; Toupet, L.; Réau, R. Electropolymerization of π-Conjugated Oligomers Containing Phosphole Cores and Terminal Thienyl Moieties: Optical and Electronic Properties. *Angew. Chem. Int. Ed.* **2000**, *39* (10), 1812–1815.
(46) Hay, C.; Vilain, D. L.; Deborde, V.; Réau, R.; Toupet, L. 2,5-Di(2-Pyridyl)Phospholes: Model Compounds for the Engineering of π-Conjugated Donor–Acceptor Co-Oligomers with a Chemically Tunable HOMO–LUMO Gap. *Chem. Commun.* **1999**, *0* (4), 345–346.
(47) Fave, C.; Cho, T.-Y.; Hissler, M.; Chen, C.-W.; Luh, T.-Y.; Wu, C.-C.; Réau, R. First Examples of Organophosphorus-Containing Materials for Light-Emitting Diodes. *J. Am. Chem. Soc.* **2003**, *125* (31), 9254–9255.
(48) Romero-Nieto, C.; Baumgartner, T. Dithieno[3,2-b:2′,3′-d]Phospholes: A Look Back at the First Decade. *Synlett* **2013**, *24* (8), 920–937.
(49) Cnops, K.; Rand, B. P.; Cheyns, D.; Verreet, B.; Empl, M. A.; Heremans, P. 8.4% Efficient Fullerene-Free Organic Solar Cells Exploiting Long-Range Exciton Energy Transfer. *Nat. Commun.* **2014**, *5*, 3406.
(50) Liu, F.; Ding, Z.; Liu, J.; Wang, L. An Organoboron Compound with a Wide Absorption Spectrum for Solar Cell Applications. *Chem. Commun.* **2017**, *53* (90), 12213–12216.
(51) Cataldo, S.; Fabiano, S.; Ferrante, F.; Previti, F.; Patanè, S.; Pignataro, B. Organoboron Polymers for Photovoltaic Bulk Heterojunctions. *Macromol. Rapid Commun.* **2010**, *31* (14), 1281–1286.
(52) Yin, X.; Chen, J.; Lalancette, R. A.; Marder, T. B.; Jäkle, F. Highly Electron-Deficient and Air-Stable Conjugated Thienylboranes. *Angew. Chem. Int. Ed.* **2014**, *53* (37), 9761–9765.
(53) Yin, X.; Liu, K.; Ren, Y.; A. Lalancette, R.; Loo, Y.-L.; Jäkle, F. Pyridalthiadiazole Acceptor-Functionalized Triarylboranes with Multi-Responsive Optoelectronic Characteristics. *Chem. Sci.* **2017**, *8* (8), 5497–5505.
(54) Frisch, M.; Trucks, G.; Schlegel, H.; Scuseria, G.; Robb, M.; Cheeseman, J.; Scalmani, G.; Barone, V.; Mennucci, B.; Petersson, G.; et al. Gaussian 16, Revision A.03. *Gaussian 16 Revis. A03 Gaussian Inc Wallingford CT* **2016**.
(55) Dennington, R.; Keith, T. A.; Millam, J. M. GaussView, Version 5. *Semichem Inc Shawnee Mission KS* **2009**.
(56) Becke, A. D. Density-Functional Exchange-Energy Approximation with Correct Asymptotic Behavior. *Phys. Rev. A* **1988**, *38* (6), 3098–3100.

(57) Lee, C.; Yang, W.; Parr, R. G. Development of the Colle-Salvetti Correlation-Energy Formula into a Functional of the Electron Density. *Phys. Rev. B* **1988**, *37* (2), 785–789.
(58) Miehlich, B.; Savin, A.; Stoll, H.; Preuss, H. Results Obtained with the Correlation Energy Density Functionals of Becke and Lee, Yang and Parr. *Chem. Phys. Lett.* **1989**, *157* (3), 200–206.
(59) Hehre, W. J.; Ditchfield, R.; Pople, J. A. Self—Consistent Molecular Orbital Methods. XII. Further Extensions of Gaussian—Type Basis Sets for Use in Molecular Orbital Studies of Organic Molecules. *J. Chem. Phys.* **1972**, *56* (5), 2257–2261.
(60) Hariharan, P. C.; Pople, J. A. The Influence of Polarization Functions on Molecular Orbital Hydrogenation Energies. *Theor. Chim. Acta* **1973**, *28* (3), 213–222.
(61) Francl, M. M.; Pietro, W. J.; Hehre, W. J.; Binkley, J. S.; Gordon, M. S.; DeFrees, D. J.; Pople, J. A. Self-consistent Molecular Orbital Methods. XXIII. A Polarization-type Basis Set for Second-row Elements. *J. Chem. Phys.* **1982**, *77* (7), 3654–3665.
(62) Binning, R. C.; Curtiss, L. A. Compact Contracted Basis Sets for Third-Row Atoms: Ga–Kr. *J. Comput. Chem.* **1990**, *11* (10), 1206–1216.
(63) Rassolov, V. A.; Pople, J. A.; Ratner, M. A.; Windus, T. L. 6-31G* Basis Set for Atoms K through Zn. *J. Chem. Phys.* **1998**, *109* (4), 1223–1229.
(64) Rassolov, V. A.; Ratner, M. A.; Pople, J. A.; Redfern, P. C.; Curtiss, L. A. 6-31G* Basis Set for Third-Row Atoms. *J. Comput. Chem.* **2001**, *22* (9), 976–984.
(65) Rutledge, L. R.; McAfee, S. M.; Welch, G. C. Design and Computational Characterization of Non-Fullerene Acceptors for Use in Solution-Processable Solar Cells. *J. Phys. Chem. A* **2014**, *118* (36), 7939–7951.
(66) Jiang, W.; Xiao, C.; Hao, L.; Wang, Z.; Ceymann, H.; Lambert, C.; Di Motta, S.; Negri, F. Localization/Delocalization of Charges in Bay-Linked Perylene Bisimides. *Chem. – Eur. J.* **2012**, *18* (22), 6764–6775.
(67) Yin, H.; Geng, Y.; Sun, G.-Y.; Su, Z.-M. Theoretical Design of Perylene Diimide Dimers with Different Linkers and Bridged Positions as Promising Non-Fullerene Acceptors for Organic Photovoltaic Cells. *J. Phys. Chem. C* **2017**, *121* (4), 2125–2134.
(68) Mercier, L. G.; Leclerc, M. Direct (Hetero)Arylation: A New Tool for Polymer Chemists. *Acc. Chem. Res.* **2013**, *46* (7), 1597–1605.
(69) Schipper, D. J.; Fagnou, K. Direct Arylation as a Synthetic Tool for the Synthesis of Thiophene-Based Organic Electronic Materials. *Chem. Mater.* **2011**, *23* (6), 1594–1600.
(70) Pouliot, J.-R.; Grenier, F.; Blaskovits, J. T.; Beaupré, S.; Leclerc, M. Direct (Hetero)Arylation Polymerization: Simplicity for Conjugated Polymer Synthesis. *Chem. Rev.* **2016**, *116* (22), 14225–14274.
(71) Lombeck, F.; Marx, F.; Strassel, K.; Kunz, S.; Lienert, C.; Komber, H.; Friend, R.; Sommer, M. To Branch or Not to Branch: C–H Selectivity of Thiophene-Based Donor–Acceptor–Donor Monomers in Direct Arylation Polycondensation Exemplified by PCDTBT. *Polym. Chem.* **2017**, *8* (32), 4738–4745.
(72) Chávez, P.; Ngov, C.; Frémont, P. de; Lévêque, P.; Leclerc, N. Synthesis by Direct Arylation of Thiazole–Derivatives: Regioisomer Configurations–Optical Properties Relationship Investigation. *J. Org. Chem.* **2014**, *79* (21), 10179–10188.
(73) Payne, A.-J.; Hendsbee, A. D.; McAfee, S. M.; Paul, D. K.; Karan, K.; Welch, G. C. Synthesis and Structure–Property Relationships of Phthalimide and Naphthalimide Based Organic π-Conjugated Small Molecules. *Phys. Chem. Chem. Phys.* **2016**, *18* (21), 14709–14719.
(74) Liu, S.-Y.; Liu, W.-Q.; Yuan, C.-X.; Zhong, A.-G.; Han, D.; Wang, B.; Shah, M. N.; Shi, M.-M.; Chen, H. Diketopyrrolopyrrole-Based Oligomers Accessed via Sequential CH

Activated Coupling for Fullerene-Free Organic Photovoltaics. *Dyes Pigments* **2016**, *134*, 139–147.

(75) Yin, X.; Guo, F.; Lalancette, R. A.; Jäkle, F. Luminescent Main-Chain Organoborane Polymers: Highly Robust, Electron-Deficient Poly(Oligothiophene Borane)s via Stille Coupling Polymerization. *Macromolecules* **2016**, *49* (2), 537–546.

(76) Pommerehne, J.; Vestweber, H.; Guss, W.; Mahrt, R. F.; Bässler, H.; Porsch, M.; Daub, J. Efficient Two Layer Leds on a Polymer Blend Basis. *Adv. Mater.* **1995**, *7* (6), 551–554.

(77) Durben, S.; Linder, T.; Baumgartner, T. Dithienophosphole-Capped π-Conjugated Oligomers. *New J. Chem.* **2010**, *34* (8), 1585–1592.

(78) Danko, M.; Andicsová, A.; Hrdlovič, P.; Račko, D.; Végh, D. Spectral Characteristics of Carbonyl Substituted 2,2′-Bithiophenes in Polymer Matrices and Low Polar Solvents. *Photochem. Photobiol. Sci.* **2013**, *12* (7), 1210–1219.

(79) Nakagawa, A.; Sakuda, E.; Ito, A.; Kitamura, N. Remarkably Intense Emission from Ruthenium(II) Complexes with Multiple Borane Centers. *Inorg. Chem.* **2015**, *54* (21), 10287–10295.

(80) Ito, A.; Kawanishi, K.; Sakuda, E.; Kitamura, N. Synthetic Control of Spectroscopic and Photophysical Properties of Triarylborane Derivatives Having Peripheral Electron-Donating Groups. *Chem. – Eur. J.* **2014**, *20* (14), 3940–3953.

(81) Kitamura, N.; Sakuda, E.; Ando, Y. Spectroscopic and Excited-State Properties of Triarylboranes and Their Transition-Metal Complexes. *Chem. Lett.* **2009**, *38* (10), 938–943.

(82) Sakuda, E.; Ando, Y.; Ito, A.; Kitamura, N. Extremely Large Dipole Moment in the Excited Singlet State of Tris{[p-(N,N-Dimethylamino)Phenylethynyl]Duryl}borane. *J. Phys. Chem. A* **2010**, *114* (34), 9144–9150.

(83) Xu, S.; Wang, X.; Feng, L.; He, Z.; Peng, H.; Cimrová, V.; Yuan, J.; Zhang, Z.-G.; Li, Y.; Zou, Y. Optimizing the Conjugated Side Chains of Quinoxaline Based Polymers for Nonfullerene Solar Cells with 10.5% Efficiency. *J. Mater. Chem. A* **2018**, *6* (7), 3074–3083.

(84) McAfee, S. M.; Payne, A.-J.; Hendsbee, A. D.; Xu, S.; Zou, Y.; Welch, G. C. Toward a Universally Compatible Non-Fullerene Acceptor: Multi-Gram Synthesis, Solvent Vapor Annealing Optimization, and BDT-Based Polymer Screening. *Sol. RRL 0* (0), 1800143.

(85) Vespa, M.; Cann, J. R.; Dayneko, S. V.; Melville, O. A.; Hendsbee, A. D.; Zou, Y.; Lessard, B. H.; Welch, G. C. Synthesis of a Perylene Diimide Dimer with Pyrrolic N–H Bonds and N-Functionalized Derivatives for Organic Field-Effect Transistors and Organic Solar Cells. *Eur. J. Org. Chem.* **2018**, *2018* (33), 4592–4599.

(86) Chen, X.; Liu, X.; Burgers, M. A.; Ye, H.; Bazan, G. C. Green-Solvent-Processed Molecular Solar Cells. *Angew. Chem. Int. Ed.* **2014**, *53* (52), 14378–14381.

(87) Byrne, F. P.; Jin, S.; Paggiola, G.; Petchey, T. H. M.; Clark, J. H.; Farmer, T. J.; Hunt, A. J.; Robert McElroy, C.; Sherwood, J. Tools and Techniques for Solvent Selection: Green Solvent Selection Guides. *Sustain. Chem. Process.* **2016**, *4*, 7.

(88) Hendsbee, A. D.; Sun, J.-P.; Law, W. K.; Yan, H.; Hill, I. G.; Spasyuk, D. M.; Welch, G. C. Synthesis, Self-Assembly, and Solar Cell Performance of N-Annulated Perylene Diimide Non-Fullerene Acceptors. *Chem. Mater.* **2016**, *28* (19), 7098–7109.

(89) Welch, G. C.; Perez, L. A.; Hoven, C. V.; Zhang, Y.; Dang, X.-D.; Sharenko, A.; Toney, M. F.; Kramer, E. J.; Nguyen, T.-Q.; Bazan, G. C. A Modular Molecular Framework for Utility in Small-Molecule Solution-Processed Organic Photovoltaic Devices. *J. Mater. Chem.* **2011**, *21* (34), 12700–12709.

(90) Wessendorf, C. D.; Schulz, G. L.; Mishra, A.; Kar, P.; Ata, I.; Weidelener, M.; Urdanpilleta, M.; Hanisch, J.; Mena-Osteritz, E.; Lindén, M.; et al. Efficiency Improvement of Solution-Processed Dithienopyrrole-Based A-D-A Oligothiophene Bulk-Heterojunction Solar Cells by Solvent Vapor Annealing. *Adv. Energy Mater.* **2014**, *4* (14), 1400266.

(91) McAfee, S. M.; Topple, J. M.; Payne, A.-J.; Sun, J.-P.; Hill, I. G.; Welch, G. C. An Electron-Deficient Small Molecule Accessible from Sustainable Synthesis and Building Blocks for Use as a Fullerene Alternative in Organic Photovoltaics. *ChemPhysChem* **2015**, *16* (6), 1190–1202.

(92) Huang, Y.; Kramer, E. J.; Heeger, A. J.; Bazan, G. C. Bulk Heterojunction Solar Cells: Morphology and Performance Relationships. *Chem. Rev.* **2014**, *114* (14), 7006–7043.

(93) McAfee, S. M.; Dayneko, S. V.; Hendsbee, A. D.; Josse, P.; Blanchard, P.; Cabanetos, C.; Welch, G. C. Applying Direct Heteroarylation Synthesis to Evaluate Organic Dyes as the Core Component in PDI-Based Molecular Materials for Fullerene-Free Organic Solar Cells. *J. Mater. Chem. A* **2017**, *5* (23), 11623–11633.

(94) Sun, Y.; Seo, J. H.; Takacs, C. J.; Seifter, J.; Heeger, A. J. Inverted Polymer Solar Cells Integrated with a Low-Temperature-Annealed Sol-Gel-Derived ZnO Film as an Electron Transport Layer. *Adv. Mater.* **2011**, *23* (14), 1679–1683.

(95) Badrou Aïch, R.; Zou, Y.; Leclerc, M.; Tao, Y. Solvent Effect and Device Optimization of Diketopyrrolopyrrole and Carbazole Copolymer Based Solar Cells. *Org. Electron.* **2010**, *11* (6), 1053–1058.

(96) Aïch, B. R.; Lu, J.; Beaupré, S.; Leclerc, M.; Tao, Y. Control of the Active Layer Nanomorphology by Using Co-Additives towards High-Performance Bulk Heterojunction Solar Cells. *Org. Electron.* **2012**, *13* (9), 1736–1741.

(97) Zheng, Y.; Goh, T.; Fan, P.; Shi, W.; Yu, J.; Taylor, A. D. Toward Efficient Thick Active PTB7 Photovoltaic Layers Using Diphenyl Ether as a Solvent Additive. *ACS Appl. Mater. Interfaces* **2016**, *8* (24), 15724–15731.

(98) Lee, T. H.; Park, S. Y.; Walker, B.; Ko, S.-J.; Heo, J.; Woo, H. Y.; Choi, H.; Kim, J. Y. A Universal Processing Additive for High-Performance Polymer Solar Cells. *RSC Adv.* **2017**, *7* (13), 7476–7482.